SAND2010-0291C

# HIGH SPEED OPTICAL FILTERING USING ACTIVE RESONANT SUBWAVELENGTH GRATINGS

A.V. Gin[i], S.A. Kemme, R.R. Boye, D.W. Peters, J.F. Ihlefeld, R.D. Briggs, J.R. Wendt, A.R. Ellis, L.H. Marshall

Sandia National Laboratories, P.O. Box 5800, Albuquerque, NM 87185

T.R. Carter, J.D. Hunker

Sandia Staffing Alliance, 2500 Louisiana Blvd. NE, Ste. 229, Albuquerque, NM 87110

S. Samora

LMATA Government Services LLC, 4209 Balloon Park Rd. NE, Ste. A, Albuquerque, NM 87109

## ABSTRACT

In this work, we describe the most recent progress towards the device modeling, fabrication, testing and system integration of active resonant subwavelength grating (RSG) devices. Passive RSG devices have been a subject of interest in subwavelength-structured surfaces (SWS) in recent years due to their narrow spectral response and high quality filtering performance. Modulating the bias voltage of interdigitated metal electrodes over an electrooptic thin film material enables the RSG components to act as actively tunable high-speed optical filters. The filter characteristics of the device can be engineered using the geometry of the device grating and underlying materials.

Using electron beam lithography and specialized etch techniques, we have fabricated interdigitated metal electrodes on an insulating layer and $BaTiO_3$ thin film on sapphire substrate. With bias voltages of up to 100V, spectral red shifts of several nanometers are measured, as well as significant changes in the reflected and transmitted signal intensities around the 1.55um wavelength.

Due to their small size and lack of moving parts, these devices are attractive for high speed spectral sensing applications. We will discuss the most recent device testing results as well as comment on the system integration aspects of this project.

**KEYWORDS:** Active Filter, Multi-color, Resonant Subwavelength Grating, Optical Device

## 1. INTRODUCTION

Spectrally tunable filters that can operate at high speeds are of interest for various imaging and spectroscopy applications. For instance, photodetectors paired with narrow band filters that can scan at high frequency through a waveband of interest may be useful in the rapid identification of specific chemical or biological species. Resonant subwavelength gratings (RSGs) are particularly attractive to serve as active filter elements due to their highly customizable narrowband reflection and transmission properties as well as the prospect of high speed operation when scaled to small device sizes. Also called corrugated gratings or guided-mode resonant filters (GMRFs), RSGs are realized using a periodic surface relief or volume grating, usually involving a dielectric material, with period less than the resonant wavelength and a typically high refractive index waveguiding layer. The effective index of the grating and waveguiding layers act to control the spectral position and width of the transmission and reflectance resonance. Typical optical response includes a characteristic narrow band reflectance with nearly perfect transmittance outside of this

[i] E-mail: agin@sandia.gov Phone: 505-284-1260

resonance band. With the proper design and when fabricated from lossless materials, RSG devices can exhibit TE and TM reflectivity at resonance of 100%. In these devices, the zero order reflected and transmitted beams are present in the far-field and higher order modes are typically suppressed by design.

Considerable previous work has been performed to understand how diffraction gratings interact with propagating beams, such as investigations by Hessel and Oliner[1]. Later research sought to leverage this effect into passive filters with very narrow reflectance and transmittance wavebands. More recently, Magnusson and Wang have expanded the knowledge of guided-mode resonances in diffraction gratings using rigorous coupled-wave theory[2,3] and have conducted experiments using dielectric grating materials.[4] Kikuta, et al suggested using a set of interdigitated conductive electrodes with a varying static voltage bias to change refractive index in an electrooptic waveguiding material.[5] However, no experimental data were published from resulting efforts. Sharon, et al has previously demonstrated an active RSG device in the near infrared utilizing a 'frame' electrode geometry and applied voltage in the growth direction. The transmitted signal was suppressed, but no wavelength shifts were demonstrated.[6]

At Sandia National Laboratories, work has progressed for the past several years on the development of resonant subwavelength grating devices. Specifically, the effects of various real-world design considerations within an array of RSG devices were investigated.[7] Additionally, we have demonstrated reflectivity of over 98% at for resonance wavelengths around 850nm in dielectric passive RSGs and described work towards an active device utilizing indium tin oxide or gold interdigitated fingers and an electrooptic thin film.[8] We have previously demonstrated an active resonant subwavelength grating device.[9] Throughout this paper we will use the 'active' label to describe a device that implements a variable voltage bias to modulate the refractive index of an electrooptic film and consequently the filter reflection/transmission spectra.

In this work, we show the latest results with active resonant subwavelength grating devices at Sandia National Laboratories. Specifically, we use an array of interdigitated metal electrodes with subwavelength pitch and $BaTiO_3$ electrooptic thin film to induce a resonance around 1.5 microns. A voltage is applied to the electrodes and resonance tuning is demonstrated. Modeling and experimental evidence indicate an induced refractive index change within the $BaTiO_3$ material. We also observe significant effects due to a non-zero loss tangent in the waveguiding film within this wavelength range.

## 2. DEVICE DESIGN AND MODELING

We used various rigorous coupled wave analysis (RCWA) simulations to design the initial active RSG structure as well as to model the experimental behavior observed from the devices. In order to maximize the electric field in the electrooptic material at relatively low voltages, we use an interdigitated metal electrode geometry as described in previous work.[9] This configuration has been shown to work at high frequencies[10], which is an eventual operational goal for fast spectroscopy utilizing these devices. Guided by theoretical simulations, the finger pitch was chosen to be 850nm with duty cycle of 30%. A dielectric $SiO_2$ film was inserted between the 325nm $BaTiO_3$ layer and metal fingers to minimize loss of the waveguide mode in the metal. Taking into account these process/geometrical variables as well as the 150nm thickness of $SiO_2$ buffer material, we can estimate the resonance position and amplitude response of the RSG device.

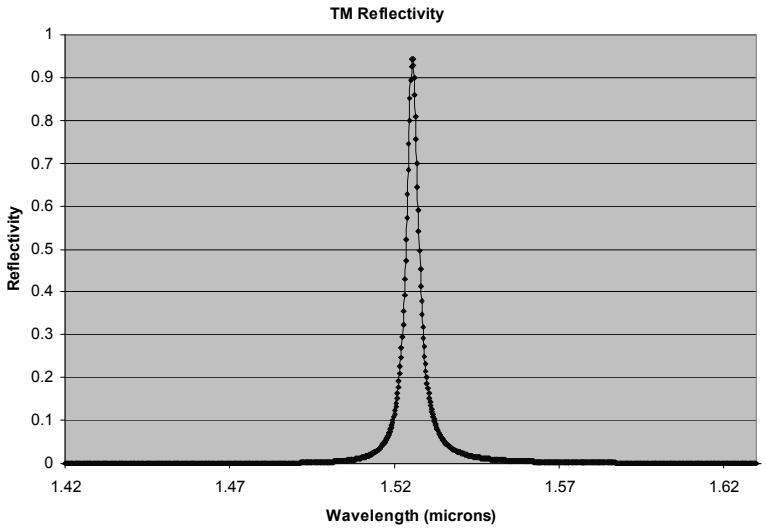


**Figure 1: Modeled TM reflectivity response at normal beam incidence using as-fabricated device materials and geometry.**

As shown in Figure 1, assuming a lossless waveguiding layer, RCWA simulations indicate a nearly 100% TM reflectivity resonance signal around 1.52µm at zero bias. The small loss in the resonance signal is caused by absorption in the metal fingers. A full width half maximum (FWHM) of 4.2nm is predicted. Additionally, we modeled the effect of various $SiO_2$ thickness from zero to 250nm as reported elsewhere.[11] As the $SiO_2$ thickness decreases to zero, the TM reflectivity peak magnitude remains relatively unchanged and the resonance is red shifted by approximately 100nm and the FWHM increases significantly. The designed 150nm $SiO_2$ thickness was a compromise between linewidth and electric field magnitude within the electrooptic film. A schematic diagram of the RSG device is shown in Figure 2.

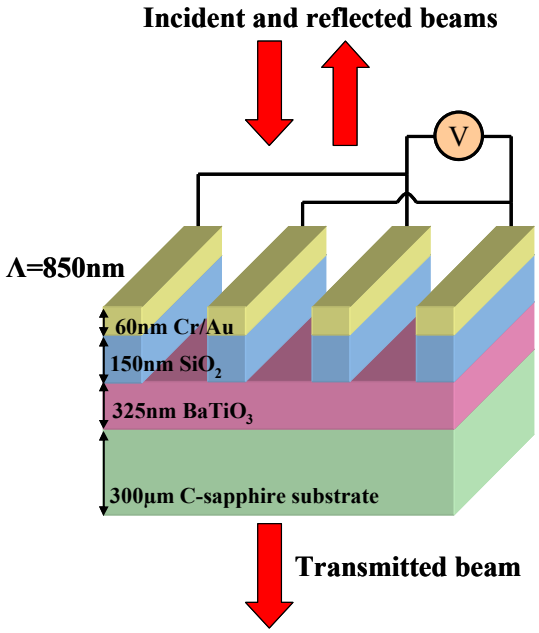


**Figure 2: Schematic drawing of an active RSG device.**

The refractive index values of the $BaTiO_3$ were taken from spectral ellipsometric measurements and the value for the sapphire substrate was assumed to be n=1.72. Modeling also aided in the design of the laboratory experiment by simulating such things as the RSG transition wavelength versus incident source angle.

## 3. MATERIAL SYNTHESIS AND CHARACTERIZATION

Perovskite ($ABO_3$) $BaTiO_3$ and $Ba_{0.5}Sr_{0.5}TiO_3$ thin films were deposited on 2" double side polished *c*-axis oriented sapphire wafers via chemical solution deposition (CSD) using a chelate chemistry.[12,13] Barium acetate or barium acetate/strontium acetate were dissolved in propionic acid to form an *A*-site precursor solution. The *B*-site precursor was formed by chelating titanium isopropoxide with 2,4 pentanedione in a 2:1 molar ratio. The *A*-site solution was added to the titanium precursor in an equimolar ratio as determined by constituent masses and the solution was diluted to 0.1 M with methanol. The solutions were deposited through a 0.2 μm filter onto the $Al_2O_3$ substrates and spin cast at 4000 RPM for 30 seconds. The samples were placed on a 250°C hotplate for 5 minutes for solvent extraction and gel consolidation. Spin casting was repeated and the films crystallized at 900°C for 30 minutes in air with 20°C/min temperature ramps. The chosen crystallization temperature is sufficient for enhanced film crystallinity while disallowing unfavorable substrate/film reactions.[14,15] Processing steps were repeated seven times resulting in ~325 nm thick films as measured by step profilometry. Additional films were prepared using rf-magnetron sputtering. $BaTiO_3$ films were deposited from a 3" $BaTiO_3$ target using a 125W cathode energy in 10 mTorr of argon. Films were deposited at room temperature and post-annealed in air to 900°C under the same conditions as described above. In this work, we focus on the CSD films. Initial sputtered film depositions indicate further process optimization is required for proper stoichiometry in the $BaTiO_3$ material.

Figure 3 shows representative X-ray diffraction patterns for CSD-derived $BaTiO_3$ and $Ba_{0.5}Sr_{0.5}TiO_3$ films deposited on (0001)-oriented $Al_2O_3$. Only peaks associated with the perovskite film and sapphire substrate were identified, which suggests that the processing conditions were appropriate to minimize film/substrate reaction phases. The film diffraction patterns are consistent with polycrystalline microstructures with no preferred orientation.

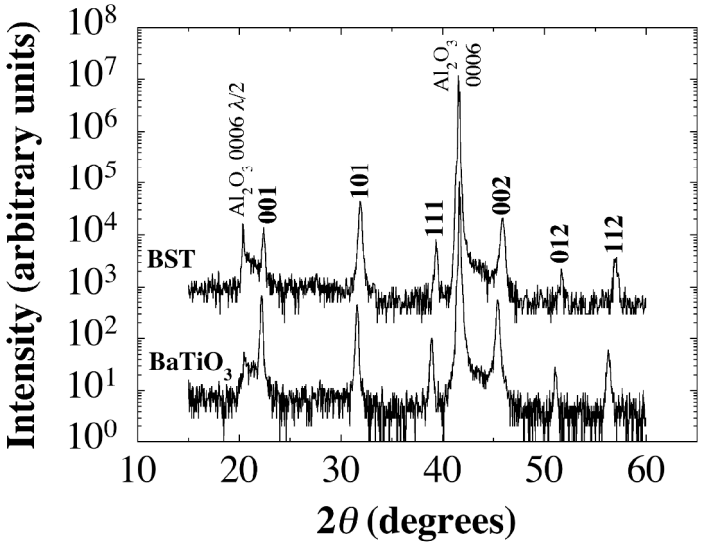


**Figure 3: X-ray diffraction patterns for 300 nm thick $BaTiO_3$ and $Ba_{0.5}Sr_{0.5}TiO_3$ thin films deposited on sapphire substrates.[9]**

Spectroscopic ellipsometry was used to measure refractive index of the deposited thin films from 900 to 1800 nm using a Woollam M2000 instrument. Figure 4 shows the corresponding refractive indices for $BaTiO_3$ and $Ba_{0.5}Sr_{0.5}TiO_3$ films. Refractive index values range between 2.225 and 2.275 over the spectral range and decrease with increasing wavelength. These values and trends with wavelength were consistent with those recorded for single crystals.[16] The absorption for both materials was less than the detectable limit of the tool within this wavelength range.

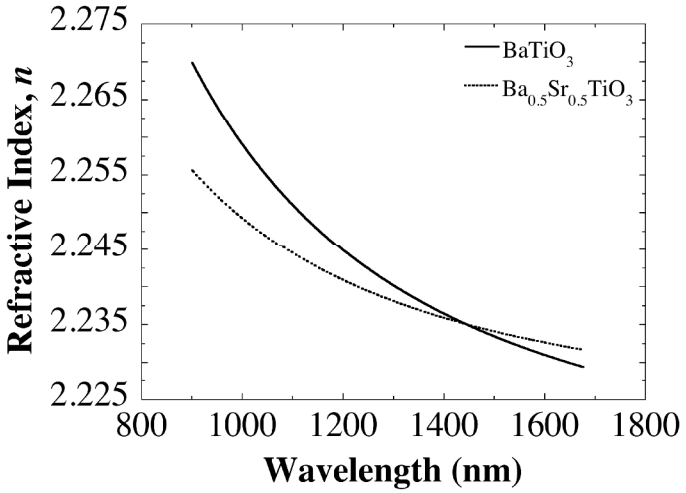


**Figure 4: Measured refractive index data for 325 nm thick $BaTiO_3$ and $Ba_{0.5}Sr_{0.5}TiO_3$ thin films deposited on sapphire substrates.[9]**

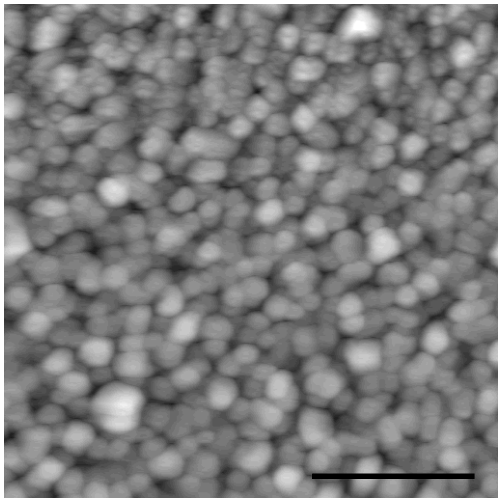

**Figure 5: A 3x3µm atomic force micrograph of a representative BaTiO3 film formed by the CSD method. The black scale bar represents 1µm.**

After material deposition, atomic force microscope (AFM) imaging was performed on $BaTiO_3$ films formed using the CSD method. In agreement with the x-ray data, the films appeared polycrystalline and average grain sizes were observed to be around 120nm as shown in Figure 5.

## 4. DEVICE FABRICATION

Following electrooptic material thin film deposition, the samples were cleaned and a 150nm $SiO_2$ film was deposited using chemical vapor deposition. Approximately 3300Å 495K C4 polymethylmethacrylate was spun and baked onto the surface of the sample. A thin metal flash layer was deposited to control charge buildup on the insulating substrate. A JEOL JBX-9300FS electron beam lithography system operating at 100kV acceleration voltage was used to expose the sample, followed by removal of the flash layer and resist development. Using a liftoff procedure, the metal electrodes were formed with 50/550 Cr/Au thickness. The electrodes were written with 850nm pitch and 30% duty cycle. Optical lithography and another metal deposition and liftoff step was performed to realize thick metal (100/3500Å Ti/Au) bus lines. Finally, a reactive ion etch was used to remove the $SiO_2$ around the electrodes using a self-aligned metal mask. Figure 6 is a scanning electron microscope image representative of an as-fabricated active RSG device.

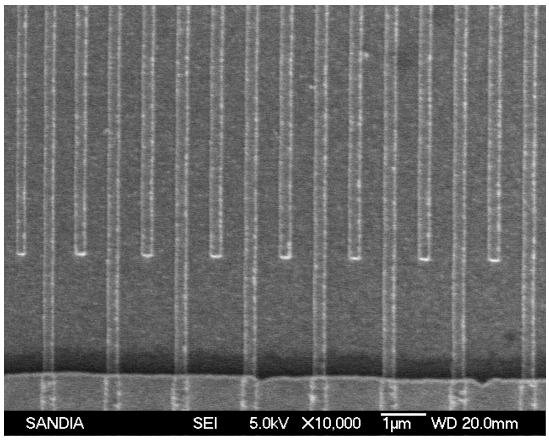


**Figure 6: Scanning electron microscope image representative of a portion of a fabricated resonant subwavelength grating device. Cr/Au electrode pitch is 850nm with a duty cycle of approximately 30%. Raised area on the bottom is the thick Ti/Au bus contact pad.**

Probe station current/voltage measurements were used to ascertain the successful fabrication of the RSG devices. The majority of devices showed the expected large (greater than a MOhm) resistance characteristics with others exhibiting varying degrees of electrical shorting most likely due to imperfect metal electrode liftoff.

## 5. EXPERIMENTAL SETUP AND DATA COLLECTION

A polarization-maintaining fiber-coupled Santec laser with output power of around 2.5mW was used as the optical source and tuned in wavelength between 1500-1580nm. A polarizing beam cube was then used to clean up the laser polarization. An aperture was interposed for beam sizing and then the optical beam was directed into a 50/50 beam splitter for reference and transmission/reflection beams. The RSG device was mounted on an XY translation/tilt/rotation stage. We show data here for an incident angle of 2 degrees from normal with respect to the device under test. A 3 degree BK7 wedge and index-matching oil were used to reduce the appearance of fringes due to multiple reflections within the sample. Large area Ge detectors measured the reflected and transmitted signals. Data for reflection and transmission were collected simultaneously and normalized to the reference beam using Lab Windows/CVI.

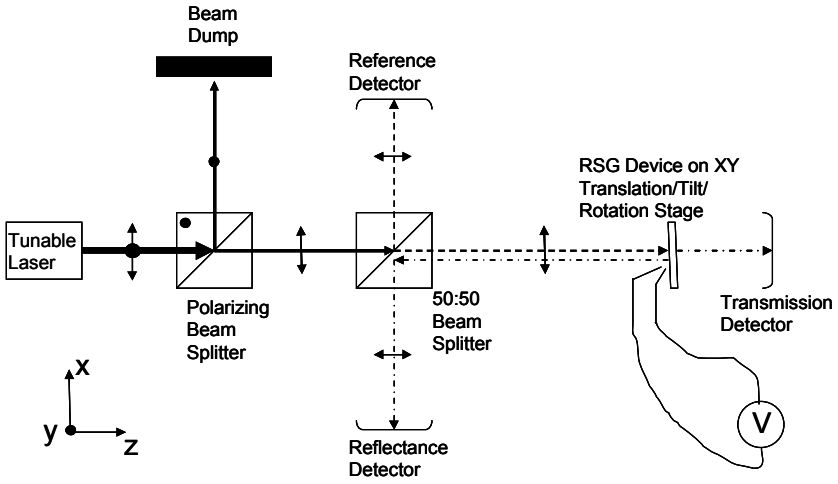


**Figure 7: Plan view schematic diagram of the RSG optical characterization setup.**

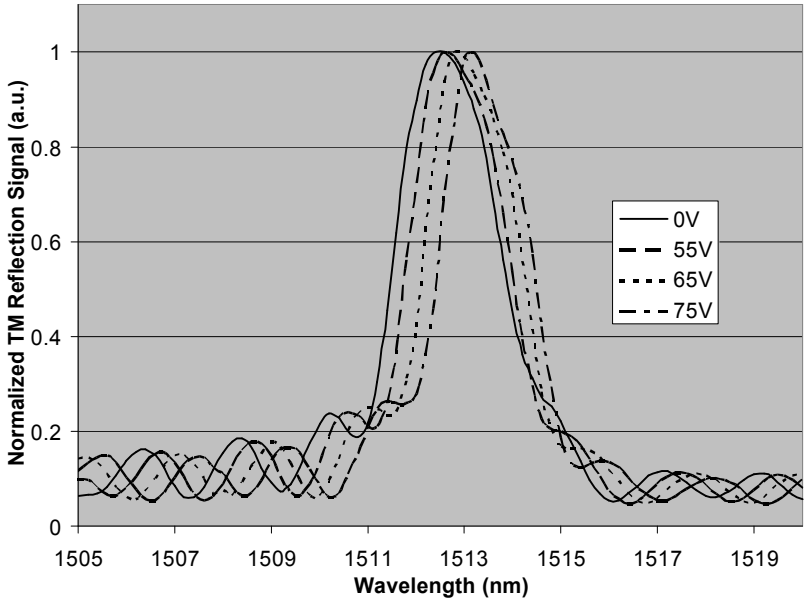


**Figure 8: Normalized TM reflection measured at several different applied voltages. Full width half maximum is around 2.6nm or thinner depending on applied voltage. Actual peak amplitudes were around 28% of reference beam.**

Normalized reflectance data from the transverse magnetic polarization is shown in Figure 8. Resonance transition is observed at about 1512.5nm at zero bias and applied bias red shifts it by a maximum of about 0.8nm. Sidelobe fringing is due to constructive/destructive interference arising from reflections off of the back surface of the sample substrate. The addition of a wedge and index matching oil helps the situation, but the remaining index difference between the BK7 material and oil with sapphire substrate allows these fringes to persist. The actual maximum of the reflected TM signal at resonance is approximately 28%. It was noted that relatively small changes (0-10°) in sample rotation with respect to incident polarization (φ) did not substantially change the magnitude or position of the reflected TM resonance signal.

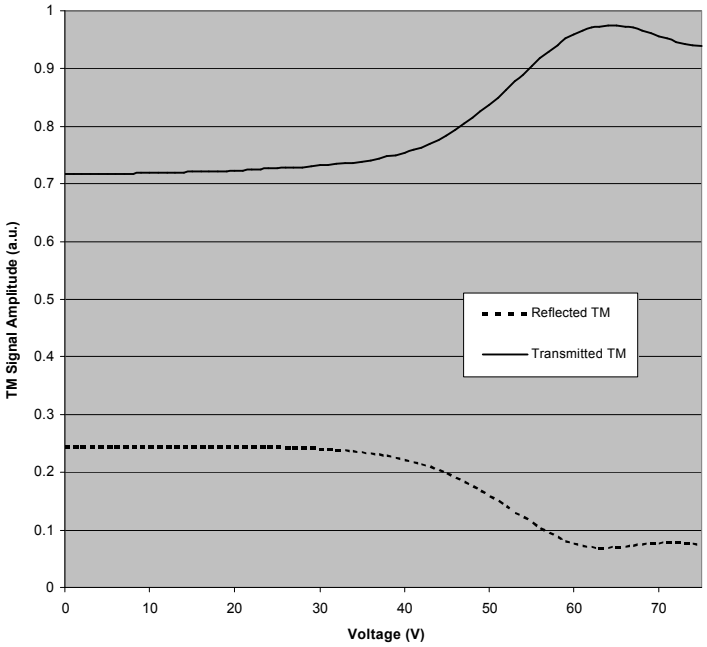


**Figure 9: Measured reflected and transmitted TM signals versus voltage at a constant source wavelength of 1512nm.**

One way to quantify the active filtering performance at a particular wavelength is shown in Figure 9. Here we used a constant laser wavelength of 1512nm and vary the applied voltage to the interdigitated fingers. We were able to modulate the reflected TM by about 20% and the transmitted TM signal by almost 30%.

## 6. ANALYSIS

We compared the experimental data for the TM reflected signal and a RCWA modeled curve as shown in Figure 10. The only fit parameter used was the loss tangent, k in the waveguiding $BaTiO_3$ layer. By adjusting k, similar signal magnitudes and FWHM were possible when compared to the actual data. In separate models, we observed that peak reflectivity and FWHM is severely affected when loss is introduced into the waveguiding layer. A best fit to experimental data was found when a value of k=0.003 was used to model the $BaTiO_3$ film. For best performance, it appears that single crystal, lossless electrooptic films are an essential component of active RSG devices.

One notable discrepancy is the wavelength shift between the two sets of curves, which we attribute to small shifts in the real part of the refractive index in the actual device material compared to the reference sample used to obtain the refractive index of the $BaTiO_3$ through ellipsometry. Additionally, very small incidence ($\theta$) angle shifts away from the modeled condition of 2° off-axis from normal can also result in wavelength shifts of this magnitude.

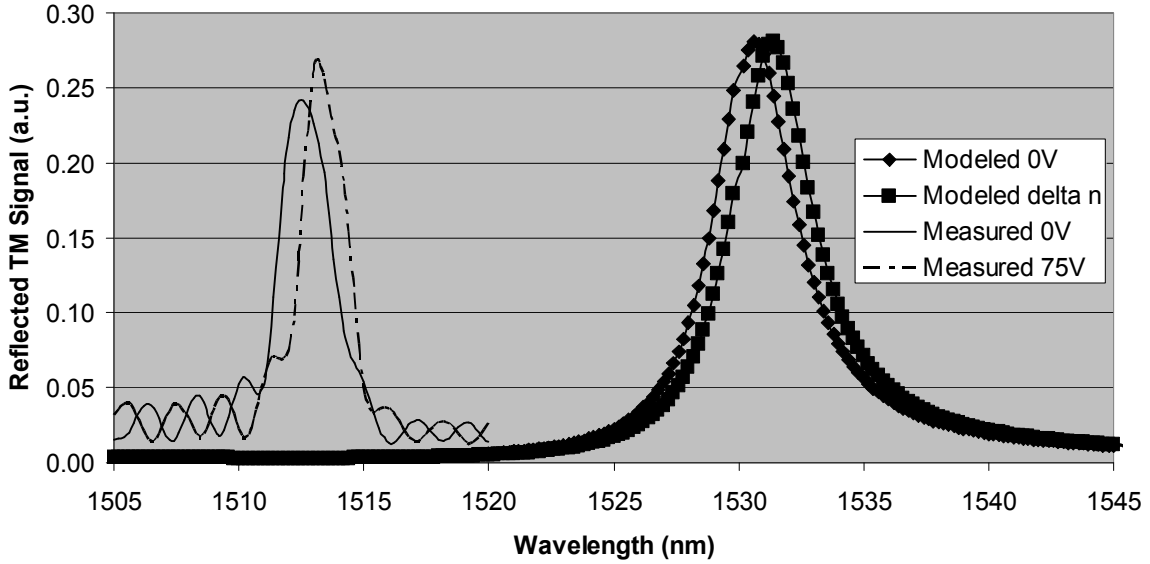


**Figure 10: Comparison of model and experimental data for reflected TM signal. The fit parameter used was loss tangent, k=0.003.**

We observed a significantly smaller FWHM in the experimental data. One possible explanation for this could be a thinner than expected $BaTiO_3$ electrooptic film or silicon dioxide layer. Both of these situations would lead to a narrower resonance waveform. By assuming a uniform change in the refractive index in the electrooptic film, we estimate a 0.0027 shift in the refractive index ($\Delta n$). This is comparable to a 0.0034 index change observed in previous experiments concentrated on the TE polarization in similar devices.[9]

Despite the fact that we are dissipating several watts of power into the device at maximum bias, it does not appear that the refractive index shift is due to temperature change in the $BaTiO_3$ (dn/dT). The literature suggests that around room temperature, refractive index in bulk $BaTiO_3$ is fairly constant until about 80C.[17] At maximum bias voltage and current, images using a FLIR infrared camera suggest that we increase the local temperature of the device under test by only a few degrees from the ambient. Further temperature-dependent spectral ellipsometry measurements with a calibrated hot stage are planned to reinforce this hypothesis.

## 7. CONCLUSION

In summary, we have described the current state of research on active resonant subwavelength gratings at Sandia National Laboratories. Namely, we have detailed the modeling, device fabrication, testing and performance analysis of these RSGs for use as narrow band active filters. Using interdigitated metal electrodes on a $BaTiO_3$ electrooptic thin film, we demonstrated refractive index modulation and red shift of the transverse magnetic reflectance and transmission resonance positions when an electric field is applied between Ti/Au electrodes. A red shift of about 1nm was observed for devices with RSG transitions around 1513nm under high voltage.

This work was performed, in part, at the Center for Integrated Nanotechnologies, a U.S. Department of Energy, Office of Basic Energy Sciences user facility. Additional support provided by the Laboratory Directed Research and Development program at Sandia National Laboratories. Sandia is a multiprogram laboratory operated by Sandia Corporation, a Lockheed Martin Company, for the United States Department of Energy's National Nuclear Security Administration under Contract DE-AC04-94AL85000.

## REFERENCES

[1] Hessel, A., Oliner, A.A., "A New Theory of Wood's Anomalies on Optical Gratings," Appl. Opt. 4(10) 1275-1297 (1965).

[2] Wang, S.S., Magnusson, R., Bagby, J.S., "Guided-mode resonances in planar dielectric-layer diffraction gratings," J. Opt. Soc. Am. A 7(8) 1470-1474 (1990).
[3] Magnusson, R., Wang, S.S., "New principle for optical filters," Appl. Phys. Lett. 61(9) 1022-1024 (1992).
[4] Liu, Z.S., Tibuleac, S., Shin, D., Young, P.P., Magnusson, R., "High-efficiency guided-mode resonance filter," Opt. Lett. 23(19) 1556-1558 (1998).
[5] Ichikawa, H., Kikuta, H., "Dynamic guided-mode resonant grating filter with quadratic electro-optic effect," J. Opt. Soc. Am. A 22(7) 1311-1318 (2005).
[6] Sharon, A., Rosenblatt, D., Friesen, A.A., Weber, H.G., Engel, H., Steingrueber, R., "Light modulation with resonant grating-waveguide structures," Opt. Lett. 21(19) 1564-1566 (1996).
[7] Peters, D.W., Kemme, S.A., Hadley, G.R., "Effect of finite grating, waveguide width, and end-facet geometry on resonant subwavelength grating reflectivity," J. Opt. Soc. Am. A 21(6) 981-987 (2004).
[8] Kemme, S.A., Boye, R.R., Peters, D.W., Nellums, R.O., "Active resonant subwavelength grating for scannerless range imaging sensors," Proc. SPIE 6469 646906 (2007).
[9] Gin, A.V., Kemme, S.A., Boye, R.R., Peters, D.W., Ihlefeld, J.F., Briggs, R.D., Wendt, J.R., Marshall, L.H., Carter, T.R., Samora, S., "Active resonant subwavelength grating devices for high speed spectroscopic sensing," Proc. SPIE 7218 721815 (2009).
[10] Ito, M., Wada, O., "Low Dark Current GaAs Metal-Semiconductor-Metal (MSM) Photodiodes Using $WSi_x$ Contacts," IEEE J. Quant. Elec. QE-22, 7, (1986).
[11] Peters, D.W., Gin, A.V., Kemme, S.A., Ihlefeld, J.F., Briggs, R.D., Wendt, J.R., Carter, T.R., Samora, S., "Active Guided-Mode Resonant Subwavelength Gratings," IPNRA (2009).
[12] Hoffmann, S., Waser, R., "Control of the morphology of CSD-prepared (Ba,Sr)$TiO_3$ thin films," J. Euro. Ceramic Soc. 19(6-7) 1339-1343 (1999).
[13] Schwartz, R.W., Clem, P.G., Voigt, J.A., Byhoff, E.R., Van Stry, M., Headley, T.J., Missert, N.A., "Control of microstructure and orientation in solution-deposited $BaTiO_3$ and $SrTiO_3$ thin films," J. Am. Ceramic Soc. 82(9) 2359-2367 (1999).
[14] Ihlefeld, J.F., Vodnick, A.M., Baker, S.P., Borland, W.J., Maria, J-P., "Extrinsic scaling effects on the dielectric response of ferroelectric thin films," J. Appl. Phys. 103 074112 (2008).
[15] Ghosh, D., "Tunable microwave devices using BST (barium strontium titanate) and base metal electrodes," Ph.D Thesis, North Carolina State University (2005).
[16] Cardona, M., "Optical properties and band structure of $SrTiO_3$ and $BaTiO_3$," Phys. Rev. 140(2A) A651-A655 (1965).
[17] Merz, W.J., "The Electric and Optical Behavior of $BaTiO_3$ Single-Domain Crystals," Phys. Rev. 76(8) 1221-1225 (1949).